Central receiver heat transfer enhancement using jet impingement with passive velocity excitation

Cite as: AIP Conference Proceedings **2126**, 030017 (2019); https://doi.org/10.1063/1.5117529
Published Online: 26 July 2019

Ken J. Craig

Central Receiver Heat Transfer Enhancement Using Jet Impingement with Passive Velocity Excitation

Ken J. Craig[1, a)]

[1]*Professor, Department of Mechanical and Aeronautical Engineering, University of Pretoria, Pretoria 0002 South Africa.*

[a)]Corresponding author: ken.craig@up.ac.za

Abstract. A new central receiver concept is being developed that attempts to trap solar rays and limit the re-radiation view factor. It has an array of hexagonal pyramid-like structures that form the absorbing surface facing the concentrated solar irradiation. Internal to these structures are concave surfaces where the heat transfer fluid impinges after emanating from jet nozzles. It therefore uses jet impingement heat transfer enhancement like the receivers proposed by Garbrecht et al and Lubkoll et al. The current paper extends previous work by the author by adding passive velocity excitation to the jet in the form of different obstructions in the pipe nozzle, as originally investigated using a cylindrical obstruction for a jet impacting on a flat plate by Uddin. Large Eddy Simulation is used to evaluate the temporal distribution of Nusselt number and velocity variation. The results of a jet with no obstruction is first compared to the experimental work of Lee et al as validation and then to those when using a cylindrical, triangular and airfoil-shaped obstruction to investigate the compromise between enhanced heat transfer and associated pressure drop. It is found that the triangular insert has the highest peak Nusselt number (4.6-fold increase over no obstruction) and 2.1 times the average Nusselt number coming at the expensive of a 60-fold increase in pressure drop. The cylindrical insert has a 2.4 times increase in maximum Nusselt number with an associated 42-fold increase in pressure drop, and although its effect is localized, the average Nusselt number increases 1.8 times. The airfoil insert considered was too streamlined to have a significant effect; its average Nusselt number being 33% higher at the expense of a 2.3 times higher pressure drop. There is therefore scope for optimizing the shape of the insert to balance the increase in convective heat transfer with the increase in pressure drop. Other methods of disturbing the flow (like introducing swirl) can also be investigated by extending the current method.

INTRODUCTION

The use of jet impingement heat transfer in solar receivers is not new. Garbrecht et al [1] suggested an absorber surface for a solar tower open receiver comprising of multiple pyramid-like structures inside which molten salt as heat transfer fluid (HTF) impinges on the internal surface of each pyramid and then in the return path comes into contact with axial fins for enhanced heat transfer. Lubkoll et al [2,3] describe an open receiver comprised of spikes which also use internal jet impingement heat transfer of pressurized air. The motivation for the external shape of the receiver in both these cases, as in the present study, is the limitation of the re-radiation view factor to the external environment. These receivers are however "open" and as such are exposed to possible convection losses, especially for windy conditions. Wang [4] uses local jet impingement to enhance the heat transfer in the annulus of a parabolic dish cavity receiver. The use of a cavity can limit both re-radiation losses as well as convection losses. The current work focuses on the development of a point-focus cavity receiver that uses ideas from Refs. 1, 2 and 3 and in addition adds a secondary reflector that acts both as a cavity and can provide an evenly-distributed absorbed solar irradiation heat flux distribution on the pyramid array absorber [5]. Figure 1 shows the components and variables defining the proposed receiver geometry.

SolarPACES 2018
AIP Conf. Proc. 2126, 030017-1–030017-10; https://doi.org/10.1063/1.5117529
Published by AIP Publishing. 978-0-7354-1866-0/$30.00

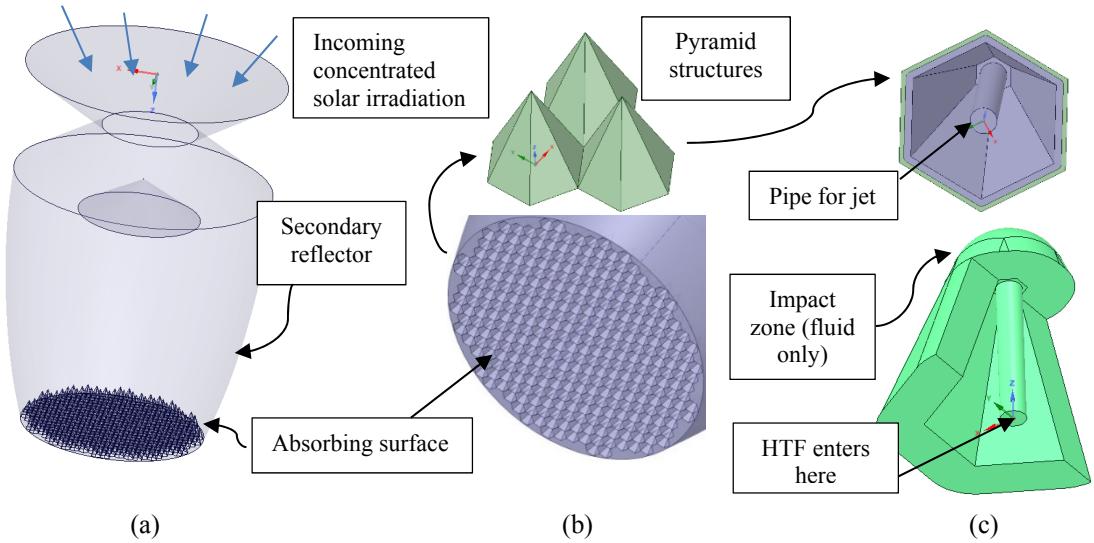

FIGURE 1. Proposed central cavity receiver (Craig et al [5]): a) absorber surface and secondary reflective surfaces, b) pyramid array structure, c) internal geometry with jet pipe and impact zone

The phenomenon of jet impingement has received widespread coverage in the heat transfer literature. Axisymmetric and quasi-axisymmetric jets are considered here. When the fluid leaves the nozzle as a free jet, ring vortices are formed that become unstable during bypass transition. Once the flow reaches the impacting surface, considered to be concave in the current work, it stagnates before flowing radially outwards. This initially laminar flow then transitions to turbulence under the influence of a favourable pressure gradient due to the curvature of the impact surface. The eventual turbulent structures cause enhanced mixing and enhanced heat transfer. Depending on the outflow condition, some re-entrainment of fluid is also possible. As for flat impingement surfaces, the famous double-hump profile in the Nusselt number distribution is observed (see, e.g., Figure 2a)). Previous work comparing Large Eddy Simulation (LES) with Reynolds-Averaged Navier-Stokes (RANS) simulations has shown that the Transition Shear-Stress-Transport (SST) 4-equation turbulence model is able to resolve the double hump phenomenon (Craig et al [5]) when simulating the time-averaged mean flow and heat transfer. These simulations were for a round jet with an essentially steady-state three-dimensional flow. Figures 2 and 3 show an excerpt of this work in the form of a Nusselt number distribution, and 3-D Transition SST and LES Nusselt contour results. The 3-D Transition SST result is axisymmetric and outperforms its 2-D counterpart (Fig.2a)). The LES result (Fig.3a)) on the other hand, displays a highly variable Nusselt number footprint, as determined by the range of scales present in the turbulent structures. Fig.3b) shows an example of these structures in the form of instantaneous iso-surfaces of the Q-criterion equal to 100 000s^{-1}, the criterion defined as $Q = \Omega^2 - S^2$ where Ω is the vorticity and S the strain rate.

To further enhance the heat transfer in the jet impact region, this study considers passive velocity excitation in the form of an obstruction placed in the pipe nozzle. This follows from the work of Uddin [6] who analyzed the effect of a circular cylinder in the nozzle with the jet impacting a flat plate. In addition, the flat impact surface is replaced with a curved impact zone for the current application of the solar receiver (Fig.1). The effect of such an obstruction is to result in unstable jet behaviour which both disturbs the axisymmetric nature of the flow described in Figs.2 and 3 and results in the need for a temporal resolution of the flow. This enhanced mixing does increase the local convection heat transfer but comes at the cost of an increased pressure drop of the jet flow. The 3-D and transient nature of the flow patterns lead to LES being considered as simulation tool in the rest of the paper.

MODEL GEOMETRY AND METHOD

The computational domain considered is depicted in Figure 4a). The concave impact surface corresponds to the impact zone shown in Fig.1c). The various obstructions (cylindrical, triangular and airfoil-shaped) are also shown in Figure 4b) to 4d).

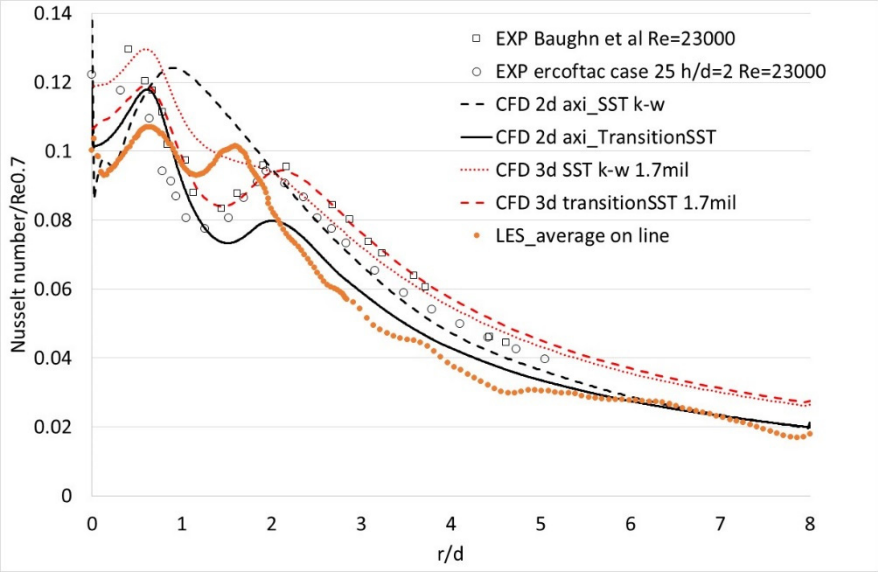

(a)

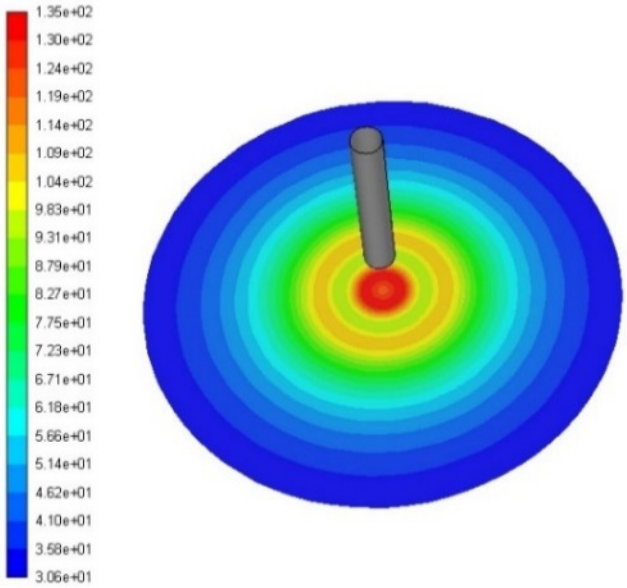

(b)

FIGURE 2. Comparison of RANS and LES results of jet impingement on a flat plate (Craig et al [5]). a) Nusselt number versus non-dimensional radial distance, b) Nusselt number contours: 3-D Transition SST turbulence model

The ratio between the jet diameter and impact sphere diameter is 0.089, with an offset distance of two jet diameters, corresponding to one of the experimental configurations in Lee et al [7] (using an empty pipe (no obstruction)) which serves as a validation case for comparison. The empty pipe case is also used as the baseline in terms of Nusselt number distribution and pressure drop when comparing the obstruction effects.

The LES method as incorporated in ANSYS Fluent v19 is used for the simulations. The subgrid scale model employed is the Wall-Adapting Local Eddy-Viscosity (WALE) method. The boundary conditions correspond to those used by Uddin [6] and Lee et al [7], with a Reynolds number of 23 000. This resulted in a uniform inlet velocity of air being V_{in}=18.255 m/s at a jet temperature, T_{in} = 40°C, when considering air as ideal gas. The corresponding pipe diameter used is 20mm. A constant heat flux of 1000W/m^2 was used as a heat flux boundary condition on the curved

wall. A standard pressure outlet was applied at the top of the computational domain (see Figure 5a)). A time step of 1E-4s was found to be sufficient in capturing the Kolmogorov integral length scale as confirmed in the results section.

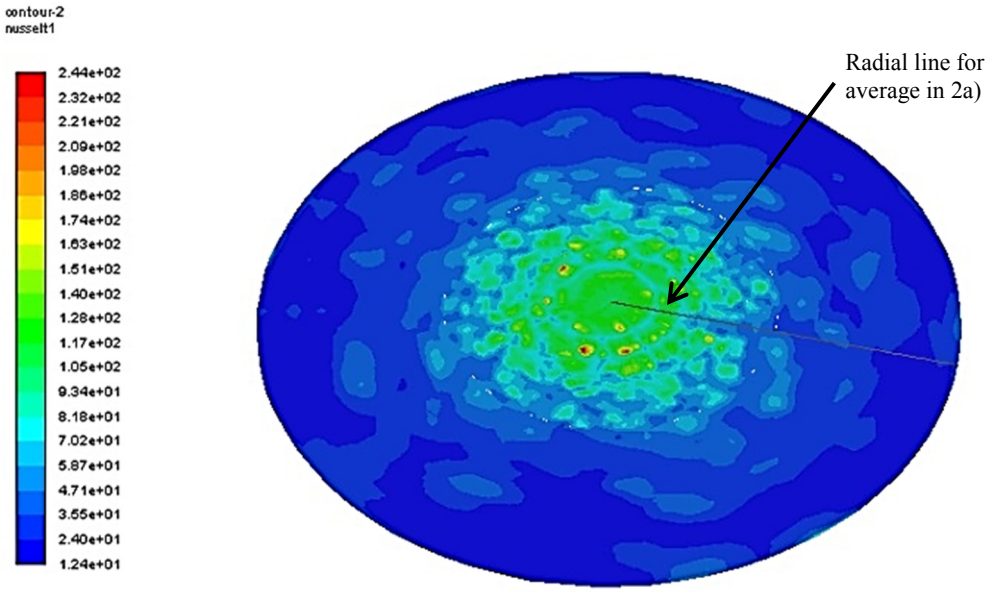

(a)

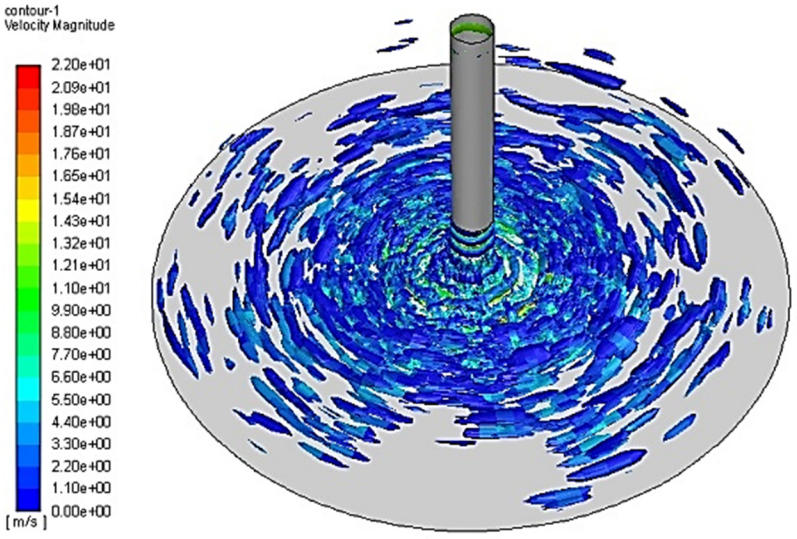

(b)

FIGURE 3. Comparison of RANS and LES results of jet impingement on a flat plate (Craig et al [5]) a) Instantaneous Nusselt number contours (LES), b) Q-criterion of 100 000s^{-1} iso-surfaces coloured by velocity magnitude

The computational domain was subdivided into sections as shown in Fig. 5 to allow for efficient mesh generation. The mesh count for the various cases varied between 6 and 6.3 million cells (see example mesh in Fig.5c)).

To compare the results to those of Uddin [6] and Lee et al [7], the resulting temperature distribution on the curved impact surface is converted to a Nusselt number using equation (1).

$$Nu = \frac{hd}{k} = \frac{\dot{q}d}{(T-T_o)k(T_o)} \tag{1}$$

where $\dot{q}$ is a constant heat source applied to the impacting surface, mimicking the solar heat source, k is the thermal conductivity (at the jet inlet temperature), T_o the inlet jet temperature and d the jet pipe diameter.

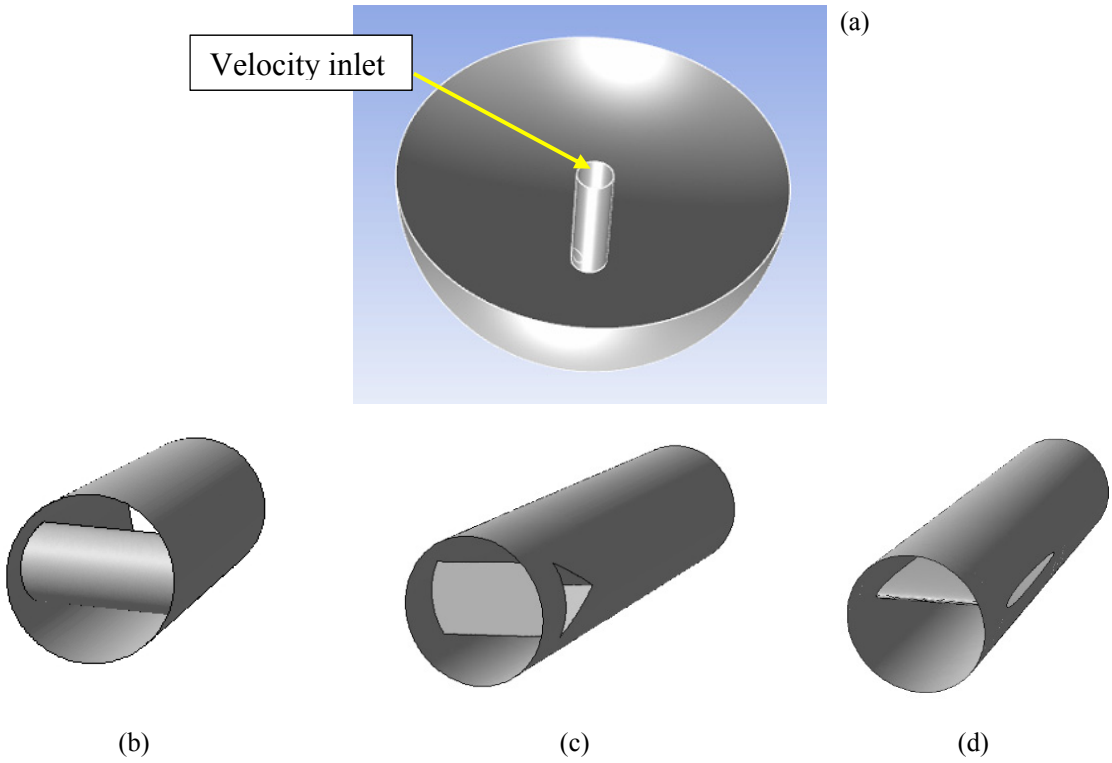

FIGURE 4. Definition of jet impact geometry. a) Concave surface and 20mm-diameter pipe from which jet emanates, b) Cylindrical obstruction (10mm diameter) in pipe nozzle, c) Triangular obstruction (10mm equilateral) in pipe nozzle, d) Airfoil obstruction in jet nozzle

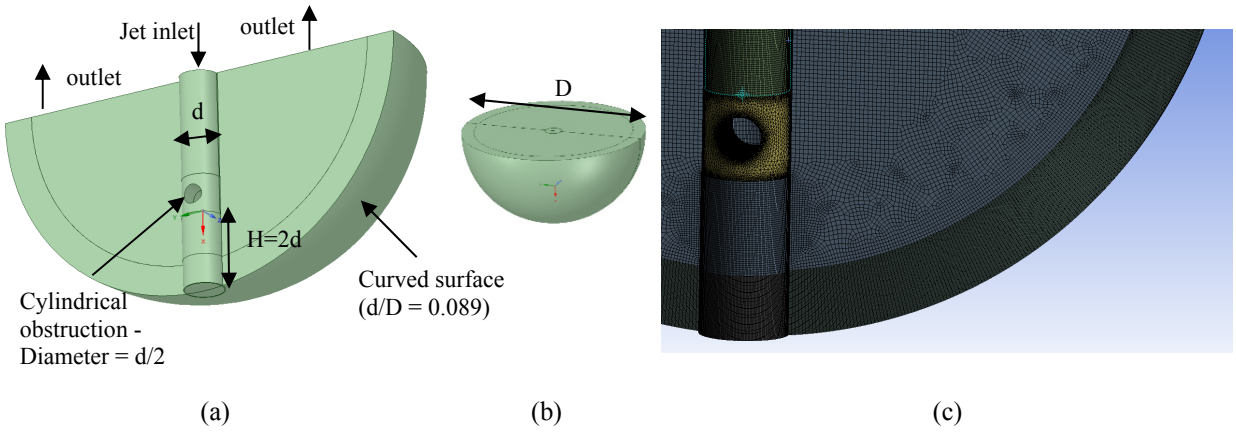

FIGURE 5. Computational domain showing a) boundary conditions and, b) mesh for cylindrical obstruction in pipe

RESULTS

Nusselt Number Distributions

Figure 6a) shows the Nusselt number versus dimensionless distance (r/d) for the case with no obstruction. It can be seen that the instantaneous LES Nusselt number on the whole impact zone straddles the experimental result of Lee et al [7] but there is some deviation in the stagnation zone and laminar region surrounding it. For reference, a 2-D axisymmetric result using the Transition SST model is also shown. With the cylindrical obstruction, the maximum Nusselt number is dramatically increased as shown in Fig.6b), being up to 2.4 times higher than without any obstruction. Higher values are obtained than for the same cylindrical obstruction impinging on a flat surface (Uddin [6]) as shown in Fig.6b). Nusselt number distributions are also provided in Fig.6 for the other two obstructions considered. The triangular obstruction results in even higher maximum Nusselt numbers (Fig.6c)), but like the cylindrical obstruction, the effect is localized. The airfoil obstruction results in good mixing on the whole impact zone with no signature laminar zone at the centre (Fig.6d)) at Nusselt numbers slightly higher than with no obstruction. In all cases, the impact zone curvature has a stabilizing effect as the flow continues to experience a favourable pressure gradient as it moves radially outward.

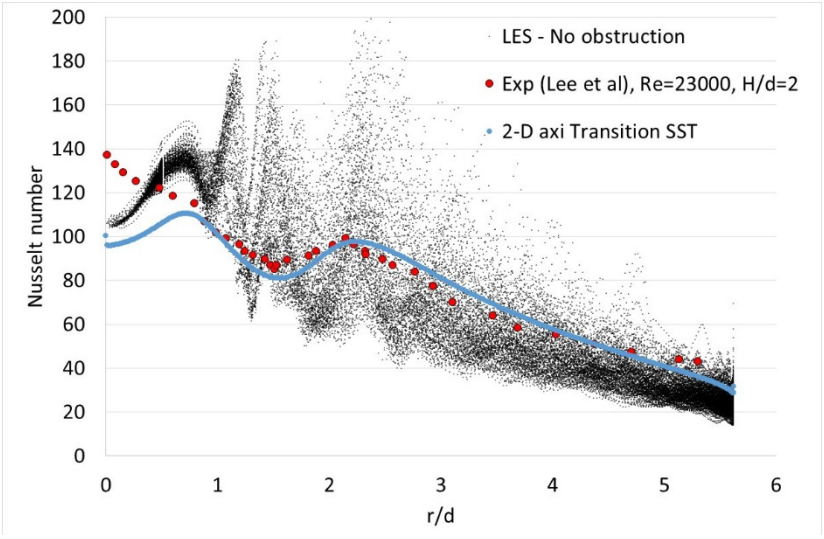

(a)

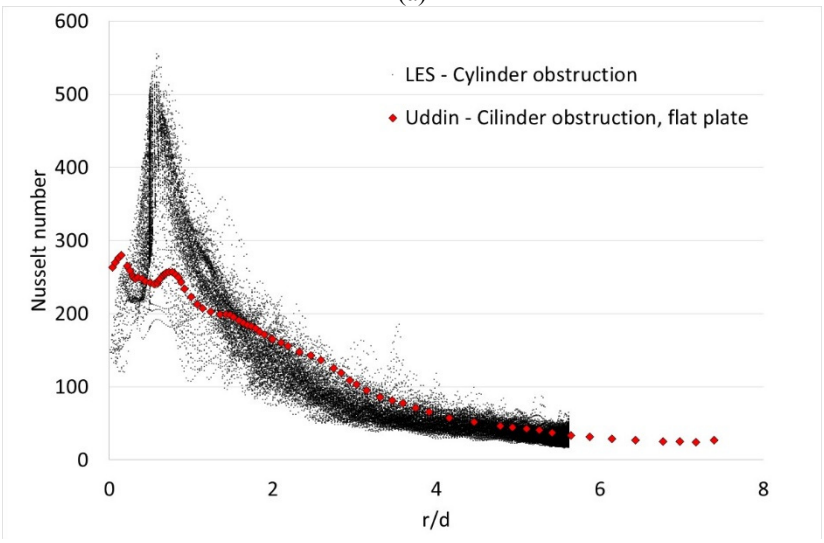

(b)

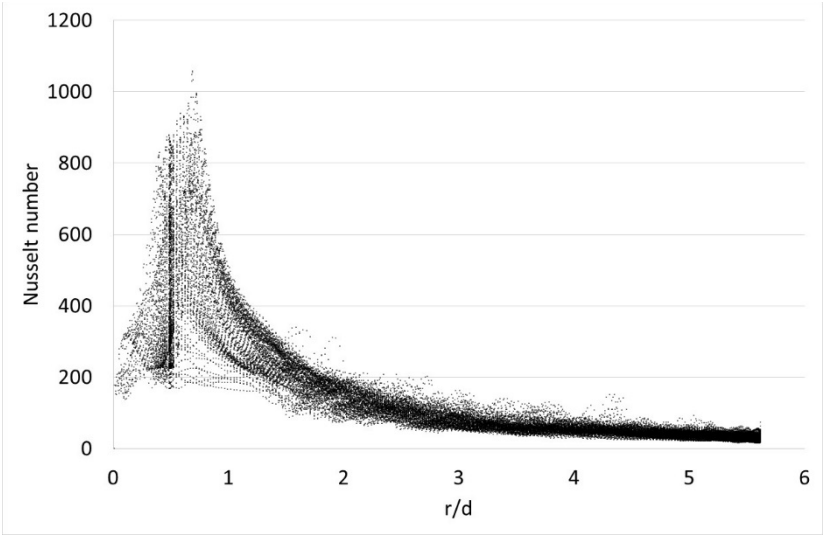

(c)

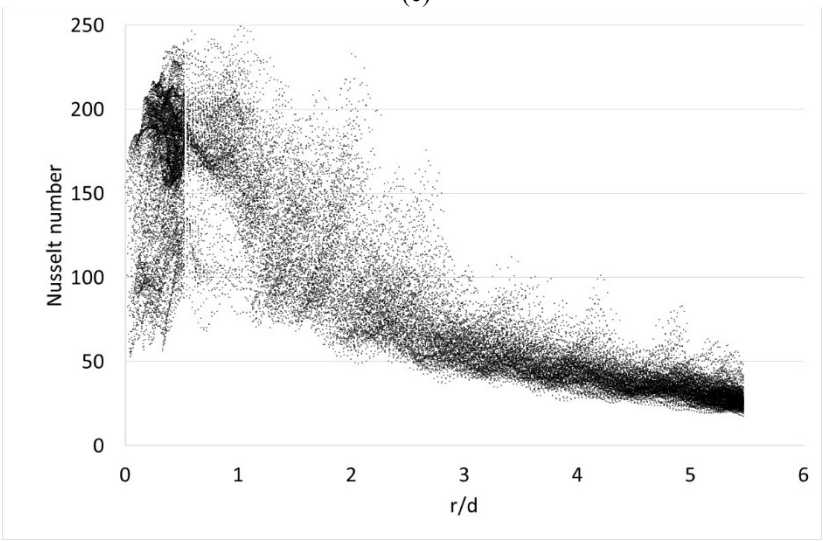

(d)

FIGURE 6. Nusselt number versus radius/jet diameter (LES data instantaneous): a) Empty pipe (no obstruction) (compared to Lee et al [7] and 2-D axisymmetric Transition SST), b) cylindrical obstruction (current curved plate vs Uddin [6] flat plate), triangular obstruction, airfoil obstruction. All cases H=2d, Re = 23 000.

Flow Patterns, Velocity Component History and Spectra

Figure 7 shows views of the velocity magnitude contours for all the obstruction cases. The effect of the obstruction is to cause a reduction in flow area with an associated increase in velocity magnitude. The obstruction also causes the flow to divide on either side of the insert, causing two jets that interact with each other. The flow pattern therefore forms a complex interaction at the impact surface. A monitor point was placed in the flow at the location shown in Fig.7a). The X-, Y- and Z-velocity components for the three cases are given in Figure 8 for a 0.1s timeframe. The Fast Fourier Transform of the largest component, the Y-velocity, is depicted in Fig.8d) for the cylindrical obstruction, confirming that the spectrum has a slope of approximately -5/3 in the inertial range (confirming Kolmogorov's theory). Note the difference in velocity scale for the airfoil obstruction compared to the other cases. This is because the airfoil does not cause the same obstruction to the flow. Also, the velocity does not fluctuate as widely for the airfoil case, implying that it is both the intensity of the jet as well as its fluctuation that leads to enhanced heat transfer.

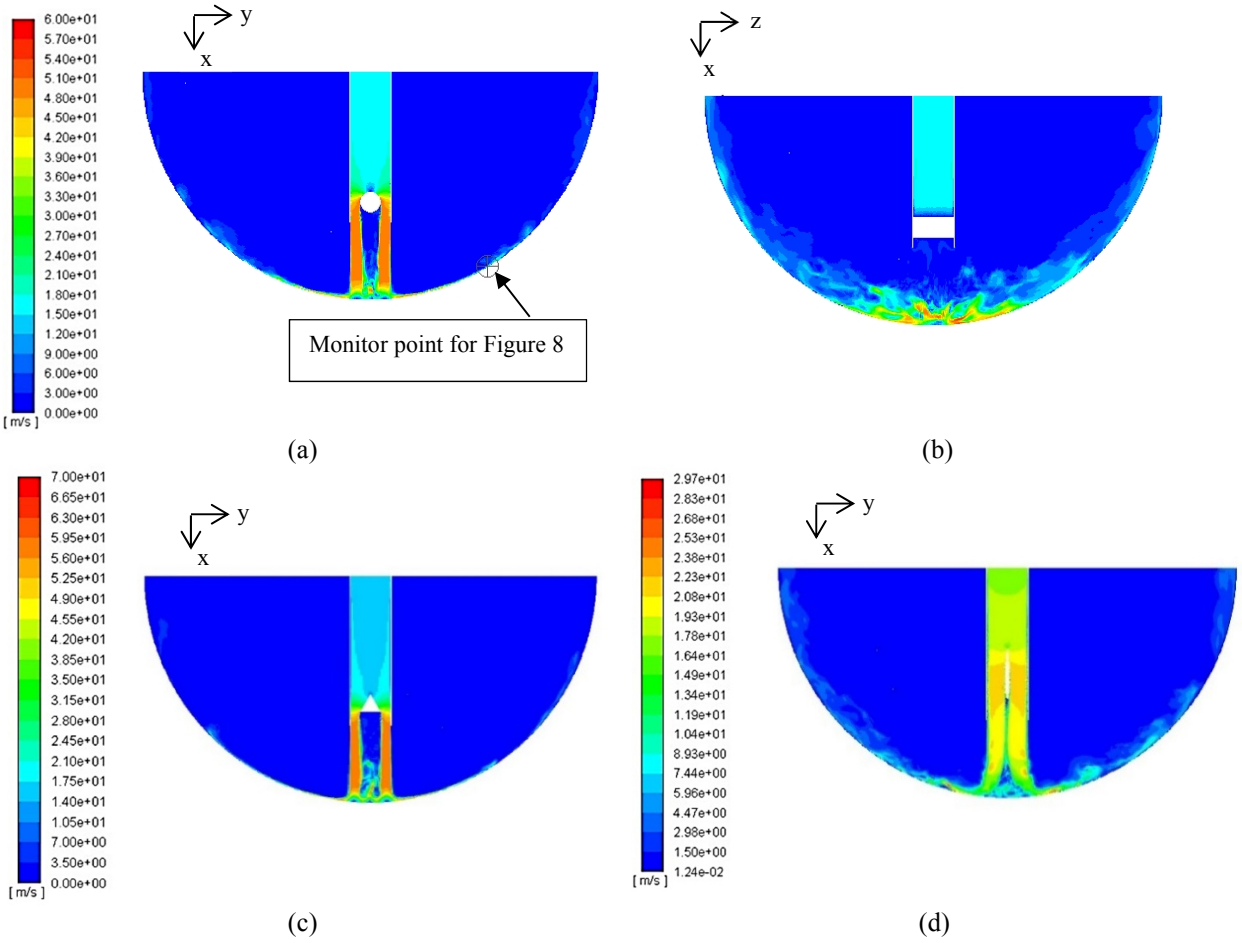

FIGURE 7. Velocity magnitude contours [m/s] for obstruction cases: a) cylindrical obstruction, z = 0 view, b) cylindrical obstruction, y = 0 view, c) triangular obstruction, d) airfoil obstruction

Q-Criterion Iso-Surfaces and Nusselt Number Contours

Figure 9 depicts Q-criterion iso-surfaces (at 100 000s^{-1}) coloured by velocity magnitude for the case of no obstruction versus a cylindrical obstruction. For no obstruction (Fig.9a), the vortex rings formed from the free jet, convect radially outward in the laminar region after which they become unstable and transition to turbulence. The disturbed jet (Fig.9b) shows an extended region of high velocity with the turbulent structures being smeared over a larger impact region. The interaction between the turbulent structures and convective heat transfer can be appreciated by comparing Fig.9 to Figure 10, where Nusselt contours are plotted on the curved wall for the three obstruction cases. The more disturbed the flow (e.g., triangular cross-section, Fig.10b), the more intense and more local is the Nusselt number peak. For the airfoil obstruction (Fig.10c)), the mixing is widespread with a large footprint of increased Nusselt number, as also exhibited in Fig.6d).

Table 1 summarizes the results of the open jet and those with the three types of obstructions. Also listed is the pressure drop over the computational domain for each case. It can be seen that the increased heat transfer comes at a significant cost of additional pressure drop, with the triangular case having up to 60 times higher pressure drop.

CONCLUSIONS

The following conclusions can be drawn from the study:

- The use of jet impingement provides a significant heat transfer enhancement that must be balanced with the increased pressure drop when designing the detail geometrical lay-out of the receiver.

- The use of obstructions in the flow to provide passive velocity excitation can be successfully evaluated using Large Eddy Simulation because of the inherent 3-D and transient nature of the flow and heat transfer phenomena.
- There is room for improvement in the detail design of the flow obstructions as well as for investigating other means of destabilizing the jet used for the enhanced heat transfer while limiting the pressure drop. Examples like imparting swirl onto the flow are topics of further work.

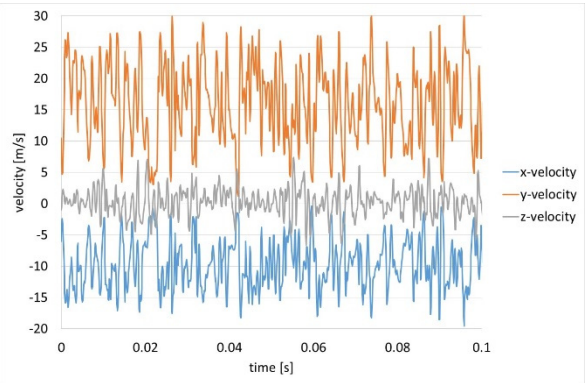

(a) Cylindrical obstruction

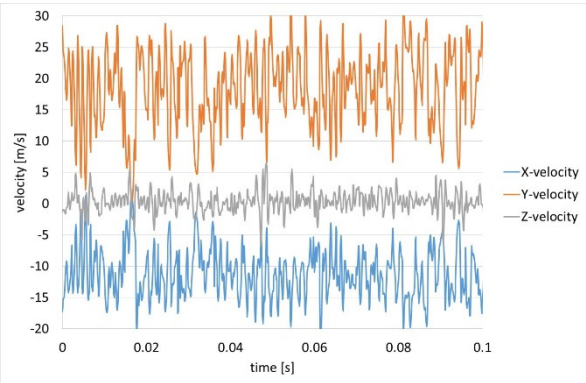

(b) Trianguar obstruction

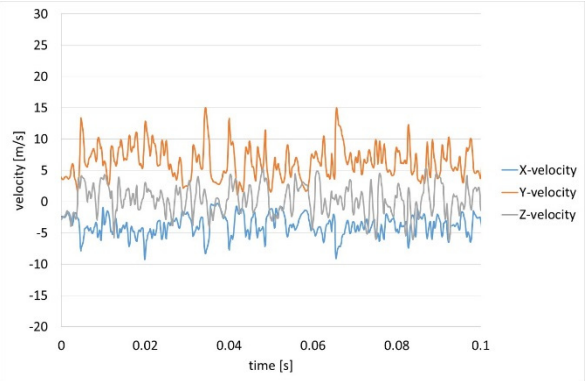

(c) Airfoil obstruction

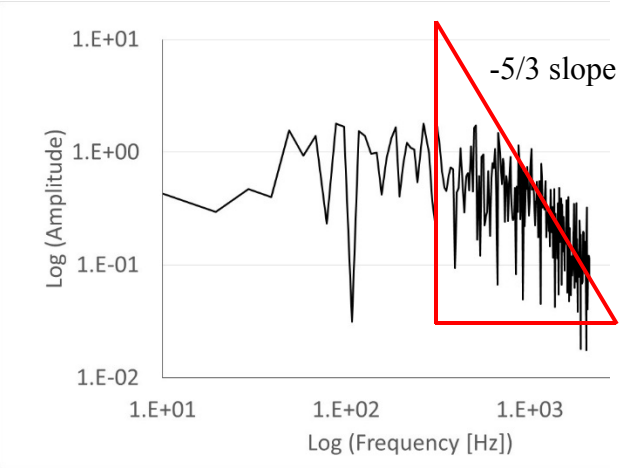

(d) FFT of Y-velocity, cylinder

FIGURE 8. Velocity time trace at monitor point (x;y;z = 0.0258; 0.0573; 0) m: a) cylindrical obstruction, b) triangular obstruction, c) airfoil obstruction, d) FFT of Y-velocity for cylindrical obstruction

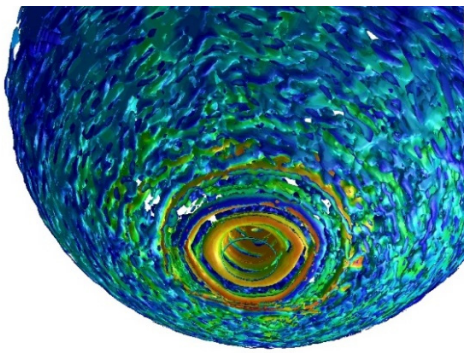

(a) No obstruction

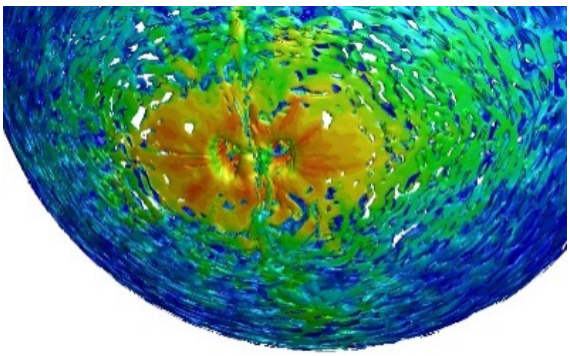

(b) Cylindrical obstruction

FIGURE 9. Q-criterion iso-surfaces (100 000s^{-1}) coloured by velocity magnitude: a) no obstruction, b) cylindrical obstruction

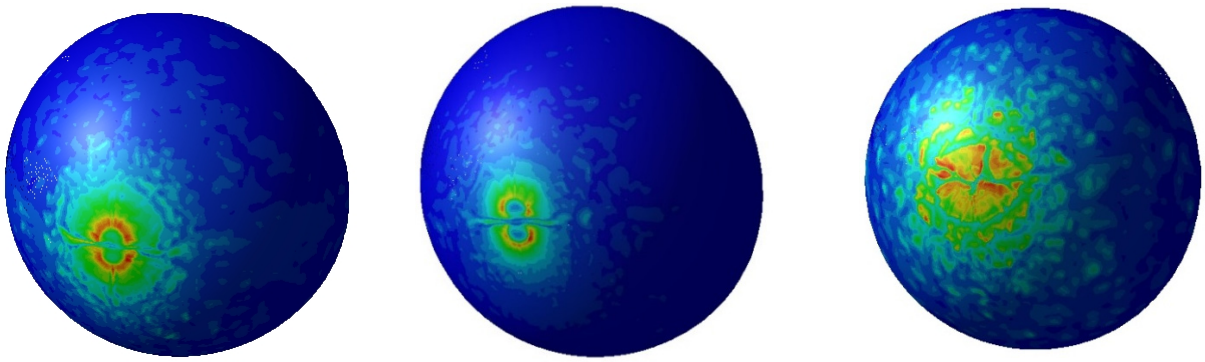

(a) Cylindrical obstruction (b) Triangular obstruction (c) Airfoil obstruction

FIGURE 10. Instantaneous Nusselt number contours on impacting surface a) cylindrical obstruction, b) triangular obstruction, and, c) airfoil obstruction

TABLE 1. Summary data illustrating the effect of the obstructions on the maximum and average Nusselt number and the pressure drop

Case	Maximum Nusselt number	Average Nusselt number	Pressure drop [Pa]
Empty pipe	232	67.0	30.3
Cylinder obstruction	556	119	1280
Triangle obstruction	1060	143	1840
Airfoil obstruction	249	86.4	70.0

ACKNOWLEDGMENTS

The author would like to acknowledge the support from the University of Pretoria (South Africa) and the South African National Research Foundation (DST-NRF Solar Spoke). The use of the Centre for High Performance Computing (CHPC) in Cape Town, South Africa, is also acknowledged.

REFERENCES

1. O. Garbrecht, F. Al-Sibai, R. Kneer and K. Wieghardt, CFD-simulation of a new receiver design for a molten salt solar power tower. Solar Energy, **90**, 94-106 (2013).
2. M. Lubkoll, T. von Backstrom, T. Harms and D. Kroger, Initial analysis on the novel Spiky Central Receiver Air Pre-heater (SCRAP) pressurized air receiver. Energy Procedia, **69**, 461-470 (2015).
3. M. Lubkoll, T.M. Harms, T.W. von Backström, Introduction to heat transfer test setup for the SCRAP receiver, AIP Conference Proceedings vol. 1850, pp. 040003 (2017), https://doi.org/10.1063/1.4984399.
4. W. Wang, Development of an impinging receiver for solar dish-Brayton systems. Ph.D. thesis, KTH Royal Institute of Technology, (2015).
5. K.J. Craig, M. Slootweg, J.P. Meyer, S.L. Robbins, J.C. Kotzé, R. Honiball, N.J.M. Grobler, E. Oosthuizen, T.J. Winterbach, W. Moll, CFD Simulation of Solar Receiver Jet Impingement Heat Transfer: RANS vs LES, Paper IHTC16-23262, Proceedings of the 16th International Heat Transfer Conference, IHTC-16, Beijing, China, August 10-15, (2018).
6. N. Uddin, Turbulence Modeling of Complex Flows in CFD, Dr. Ing. Thesis, Faculty of Aerospace Engineering and Geodesy, University of Stuttgart, (2008).
7. D.H. Lee, Y.S., Chung, Y.S. Won, The effect of concave surface curvature on heat transfer from a fully developed round impinging jet, Int J. Heat Mass Transfer, **42**, 2489-2497 (1999).